

Antagonistic in-plane resistivity anisotropies from competing fluctuations in underdoped cuprates

Michael Schütt and Rafael M. Fernandes

School of Physics and Astronomy, University of Minnesota, Minneapolis 55455, USA

One of the prime manifestations of an anisotropic electronic state in underdoped cuprates is the in-plane resistivity anisotropy $\Delta\rho \equiv (\rho_a - \rho_b)/\rho_b$. Here we use a Boltzmann-equation approach to compute the contribution to $\Delta\rho$ arising from scattering by anisotropic charge and spin fluctuations, which have been recently observed experimentally. While the anisotropy in the charge fluctuations is manifested in the correlation length, the anisotropy in the spin fluctuations emerges only in the structure factor. As a result, we find that spin fluctuations favor $\Delta\rho > 0$, whereas charge fluctuations promote $\Delta\rho < 0$, which are both consistent with the doping dependence of $\Delta\rho$ observed in $\text{YBa}_2\text{Cu}_3\text{O}_7$. We also discuss the role played by CuO chains in these materials, and propose transport experiments in strained $\text{HgBa}_2\text{CuO}_4$ and Nd_2CuO_4 to probe directly the different resistivity anisotropy regimes.

The existence of a sizable in-plane electronic anisotropy in different families of underdoped cuprates has been established by a variety of experimental probes, such as transport measurements [1–3], x-ray [4, 5] and neutron scattering [6, 7], and scanning tunneling microscopy [8]. Consonant with the proposal of electronic nematic order [9–12], in which the point group symmetry of the system is lowered spontaneously by electronic degrees of freedom, these experiments provide invaluable information for the hotly debated topic of whether any symmetries are broken in the pseudogap phase [13, 14]. To elucidate the relevance of these anisotropic properties to the phase diagram of the cuprates, it is fundamental to establish their microscopic origin. In this regard, a useful benchmark for theoretical proposals is the in-plane resistivity anisotropy $\Delta\rho \equiv (\rho_a - \rho_b)/\rho_b$, which was measured in the seminal work [1] across the phase diagram of $\text{YBa}_2\text{Cu}_3\text{O}_7$ (YBCO). The moderate values of the resistivity anisotropy that were observed experimentally, $\Delta\rho \lesssim 1.5$, are difficult to reconcile with a scenario in which metallic static stripes [15, 16] order in an insulating background. Instead, they seem to be more compatible with fluctuations that break the tetragonal symmetry of the system [10, 17].

Interestingly, neutron and x-ray measurements in underdoped YBCO have unveiled the onset of anisotropic charge and spin fluctuations at temperatures comparable to those marking the onset of $\Delta\rho$. Refs. [6, 7] found that the dynamic spin susceptibility $\chi_S(\mathbf{q}, \omega)$ in the vicinity of the magnetic ordering vector $\mathbf{Q}_S = (\pi, \pi)$ becomes strongly anisotropic as temperature is lowered, eventually giving rise to incommensurate peaks along the a direction only, and to long-range spin-density wave (SDW) order at low temperatures. More recently, it was reported that the charge susceptibility $\chi_C(\mathbf{q}, \omega)$ is also anisotropic, with fluctuations peaked at the ordering vector $\mathbf{Q}_{C,b} = Q_C \hat{\mathbf{b}}$ stronger than the fluctuations peaked at the 90° -rotated ordering vector $\mathbf{Q}_{C,a} = Q_C \hat{\mathbf{a}}$ [4, 5, 18, 19]. At high magnetic fields, superconductivity is destroyed and these fluctuations are believed to give

rise to charge-density wave (CDW) order [20, 21]. Interestingly, the SDW and CDW fluctuations seem anticorrelated in the phase diagram of YBCO [4, 19] (see Fig. 1): while the anisotropic spin fluctuations dominate the hole-doping concentration range $0.05 \lesssim p \lesssim 0.08$, the anisotropic charge fluctuations are observed predominantly in the $0.09 \lesssim p \lesssim 0.13$ range.

In this paper, we calculate the resistivity anisotropy due to the scattering by the anisotropic charge and spin fluctuations observed in Refs. [4–6] and compare it qualitatively with the resistivity anisotropy measurements of Ref. [1]. Because our focus is on the sign of $\Delta\rho \equiv (\rho_a - \rho_b)/\rho_b$ and on its dependence on the charge and spin correlation lengths ξ_C and ξ_S , respectively, we employ a Boltzmann equation approach. We find that while scattering by charge fluctuations yields $\Delta\rho < 0$ and $|\Delta\rho| \propto \xi_C^2$, scattering by spin fluctuations gives $\Delta\rho > 0$ and $|\Delta\rho| \propto \ln \xi_S$. These different behaviors arise from the fact that the former is governed by the Fermi velocity at the CDW hot spots, whereas the latter is sensitive to the curvature of the Fermi surface near the SDW hot spots. We discuss the key role played by the CuO chains present in YBCO, which act effectively as a conjugate field to the nematic order parameter, selecting the experimentally-observed fluctuation anisotropies. Our findings are consistent with the resistivity anisotropy measurements in YBCO, and in particular with the doping dependence of $\Delta\rho$ in the range $0.05 \lesssim p \lesssim 0.15$.

Our focus here is not on the mechanism responsible for the anisotropic CDW and SDW fluctuations – in fact, several models for nematicity in the cuprates have been proposed [9, 22–30]. Instead, we assume spontaneous nematic order and adopt a phenomenological approach in which the low-energy properties of the CDW and SDW susceptibilities are extracted from the scattering experiments [4–6]. Following previous works [29, 31–34], we consider the CDW ordering vectors $\mathbf{Q}_{C,i}$ that connect the magnetic hot spots of the Fermi surface [35], according to Fig. 2. We note however that small changes in the positions of the CDW hot spots do not affect our conclu-

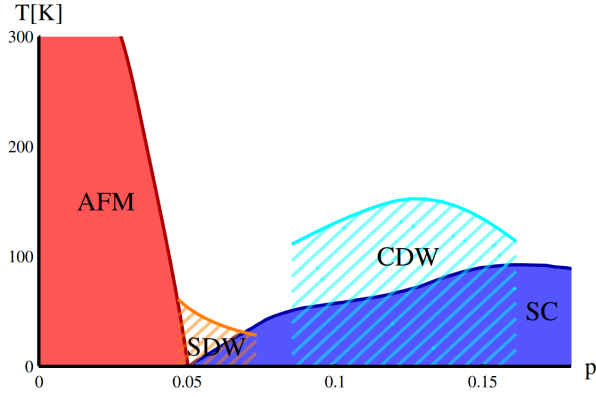


FIG. 1. Schematic phase diagram of the underdoped cuprates. Long-range incommensurate metallic spin-density wave (SDW) order sets in at low temperatures, next to the Mott insulating anti-ferromagnetic (AFM) phase, but its anisotropic fluctuations persist to higher temperatures. Charge-density wave (CDW) fluctuations, with no long-range order, are observed near the $p = 0.125$ concentration, where superconductivity (SC) is suppressed.

sions. Because $\mathbf{Q}_{C,i}$ and \mathbf{Q}_S connect states at the Fermi level, the CDW and SDW dynamics are dominated by Landau damping, i.e. $\chi_\alpha^{-1}(\mathbf{q}, \omega) = \chi_\alpha^{-1}(\mathbf{q}) - i\omega/\Gamma_\alpha$ and $\alpha = C, S$, with $\Gamma_{C/S} \propto v_F Q_{C/S}$, where v_F is the Fermi velocity. The anisotropy of the fluctuations is manifested in their static components, which, according to the experimental observations, can be modeled as:

$$\chi_{C,i}^{-1}(\mathbf{q} + \mathbf{Q}_{C,i}) = \xi_C^{-2}(1 \pm \eta_C) + q^2 \quad (1)$$

$$\chi_S^{-1}(\mathbf{q} + \mathbf{Q}_S) = \xi_S^{-2} + (1 + \eta_S)q_x^2 + (1 - \eta_S)q_y^2 \quad (2)$$

where the upper (lower) sign in the first equation refers to $i = a$ ($i = b$). Hereafter, $\hat{\mathbf{x}} \parallel \hat{\mathbf{a}}$, $\hat{\mathbf{y}} \parallel \hat{\mathbf{b}}$, and all lengths are measured in units of the lattice constant. Fig. 2 displays the contour plots of the susceptibilities, highlighting their anisotropic features: while the anisotropy of the CDW fluctuations is manifested as different correlation lengths [29, 36, 37], $\eta_C = (\xi_{C,a}^{-2} - \xi_{C,b}^{-2})/2\xi_C^{-2}$, the anisotropy of the SDW fluctuations is manifested only on its form factor via the dimensionless parameter η_S . When $|\eta_S| > 1$, the SDW develops an incommensurability along either a ($\eta_S < 0$) or b ($\eta_S > 0$). Thus, both η_S and η_C are Ising-nematic order parameters and the anisotropic resistivity obeys, by symmetry, $\Delta\rho = C_S\eta_S + C_C\eta_C$. Because our main goal is to establish the sign of the pre-factors C_S and C_C , hereafter we consider the regime $\eta_{S,C} \ll 1$.

Because macroscopic samples will be divided in equal-weight domains of $\eta_{S,C}$ and $-\eta_{S,C}$, one would not expect to observe anisotropic properties which average over the entire sample, such as $\Delta\rho$. This issue can be avoided if fields that explicitly break the tetragonal symmetry and select one domain over the other are present. In terms of a Ginzburg-Landau functional, they can be recast in

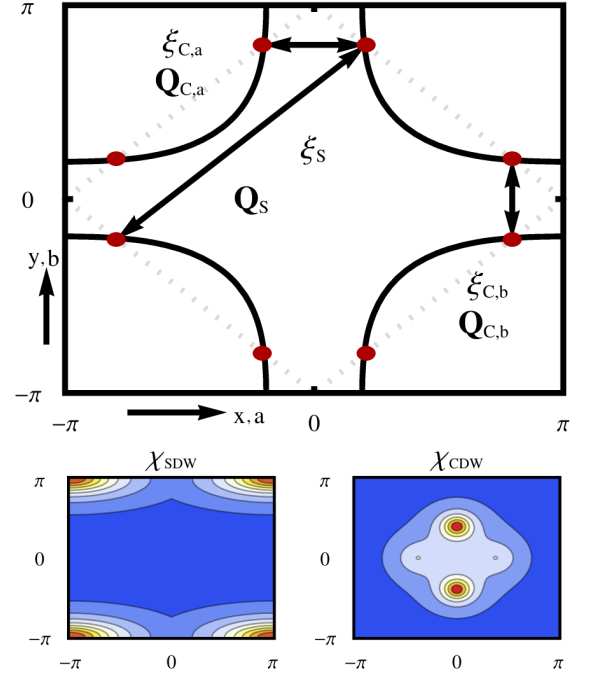


FIG. 2. (upper panel) Schematic representation of the scattering by charge and spin fluctuations. The red dots are the magnetic hot spots. Here, $\mathbf{Q}_{C,a(b)} = Q_C \hat{\mathbf{a}}(\hat{\mathbf{b}})$ and $\mathbf{Q}_S = (\pi, \pi)$ correspond to the CDW/SDW ordering vectors, and $\xi_{C,S}$ to the CDW/SDW correlation lengths. (lower panel) Contour plots of the CDW and SDW susceptibilities given by Eq. (1) across the first Brillouin zone, with $\eta_S < 0$ and $\eta_C > 0$, in accordance to experiments in YBCO.

terms of the conjugate fields h_C and h_S :

$$F[\eta_S, \eta_C] = F_0[\eta_S, \eta_C] - h_C \eta_C - h_S \eta_S \quad (3)$$

where the functional F_0 depends only on even powers of $\eta_{S,C}^2$ and $\eta_S \eta_C$. In tetragonal cuprates such as $\text{HgBa}_2\text{CuO}_4$ and Nd_2CuO_4 the symmetry-breaking field needs to be externally applied in the form of uniaxial strain. However, in detwinned YBCO, the presence of unidirectional CuO chains makes it orthorhombic, with the b direction parallel to the CuO chains [38, 39]. Thus, the small orthorhombic distortion acts effectively as an external field that selects one type of domain [40].

To verify whether this picture correctly captures the signs of η_S and η_C observed experimentally in YBCO, namely $\eta_S < 0$ and $\eta_C > 0$, we computed the signs of the effective fields $h_{C,S}$ generated by the coupling between the CuO chains and the CuO_2 planes via evaluation of the non-interacting polarization bubble $\Pi(\mathbf{q}, \omega)$ for a tight-binding model containing the chains and the planes [38, 39] (see supplementary material[41]). Because the contribution of the chains to the susceptibilities (1) is given by $\tilde{\chi}_\alpha^{-1}(\mathbf{q}) - \chi_\alpha^{-1}(\mathbf{q}) = -\Pi(\mathbf{q})$, where $\tilde{\chi}$ is the susceptibility in the presence of the conjugate fields induced by the chains, it is straightforward to extract the

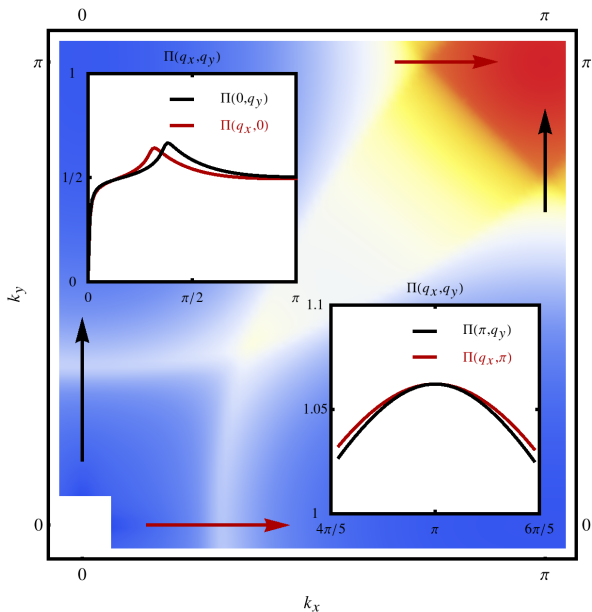


FIG. 3. (color online) Color plot of the polarization bubble $\Pi(\mathbf{q})$ across the first Brillouin zone in the presence of a non-zero coupling between the CuO chain and the CuO₂ plane. The insets show the high-symmetry cuts, indicated by the arrows, near the CDW ordering vectors ($\Pi(q_x, 0)$ and $\Pi(0, q_y)$), and near the SDW ordering vector ($\Pi(\pi, q_y)$ and $\Pi(q_x, \pi)$).

fields $h_{C,S}$. In Fig. 3 we plot $\Pi(\mathbf{q})$ across the first Brillouin zone, and present in the inset cuts along the high-symmetry directions $(q_x, 0)$, $(0, q_y)$, $(\pi + q_x, \pi)$ and $(\pi, \pi + q_y)$.

First, we note that the peaks along the 90°-related cuts $\Pi(q_x, 0)$ and $\Pi(0, q_y)$ are different, with the peak along the q_y axis (parallel to b) stronger, which corresponds to a larger correlation length around the $\mathbf{Q}_{C,b}$ ordering vector, $\xi_{C,b} > \xi_{C,a}$. Therefore, the effect of the chains can be recast in terms of a positive conjugate field $h_C > 0$ that selects the $\eta_C > 0$ domain, in agreement with the x-ray observations in YBCO [4, 5]. Meanwhile, a cut along the a and b axes centered at the $\mathbf{Q}_S = (\pi, \pi)$ ordering vector gives $\Pi(\pi + q_x, \pi) - \Pi(\pi, \pi) = -\alpha_x q_x^2$ and $\Pi(\pi, \pi + q_y) - \Pi(\pi, \pi) = -\alpha_y q_y^2$, with $\alpha_x < \alpha_y$. Thus, comparison with Eqs. (1) reveals that the chains act as a negative conjugate field $h_S < 0$, which selects the $\eta_S < 0$ domain, as also observed experimentally in YBCO via neutron scattering [6, 7]. Note that, as pointed out in Ref. [1], even though the chains contribute to $\Delta\rho$, they cannot alone explain the resistivity anisotropy behavior, since $\Delta\rho$ has a non-monotonic variation as doping decreases, whereas the degree of chain order decreases continuously with decreasing p .

Having established the form of the anisotropic SDW and CDW susceptibilities, we now compute the resistivity anisotropy arising from the scattering of electrons by these fluctuations. Because we focus on the sign of $\Delta\rho$

for small $\eta_{C,S}$, it is appropriate to employ a semi-classical Boltzmann approach [42–44], since the smallness of $\eta_{C,S}$ allows for a perturbative treatment of the collision kernel, even if the SDW and CDW coupling constants are not necessarily small. Furthermore, the observations of quantum oscillations [2], of a T^2 behavior in the resistivity [45], of the validity of Kohler’s rule [46], and of a ω^2 behavior in the ac conductivity [47] suggest that quasi-particles are well-defined in the doping range of interest. We emphasize that our focus is in the underdoped regime where $\xi_{S,C}$ remains finite, and the system is near a finite-temperature nematic phase transition. Near a putative nematic quantum critical point, the quasi-particle concept is compromised, and other approaches may be more appropriate [48–50].

Besides the inelastic scattering by CDW and SDW fluctuations, electrons are also scattered elastically by impurities (see also Refs. [51, 52]). Here, we consider the limit where the impurity potential provides the dominant scattering mechanism, which is always true at low enough temperatures. Alternatively, similar results can be obtained in the limit where scattering by isotropic fluctuations is dominant. We avoid the extremely low-temperature regime, where weak-localization and Fermi-velocity renormalization effects may be important. In the impurity-dominated regime [42, 43], the solution of the Boltzmann equation yields the resistivity anisotropy (see supplementary material):

$$\rho_a - \rho_b = \rho_0 \frac{\sum_\alpha (I_{\text{fluct}}^\alpha [h_x/\tau] - I_{\text{fluct}}^\alpha [h_y/\tau])}{I_{\text{imp}} [h/\tau]} \quad (4)$$

with the collision integrals:

$$I[h_j] = \frac{1}{2\hbar} \int_{\mathbf{p}, \mathbf{p}'} \mathcal{K}(\mathbf{p}, \mathbf{p}') (h_j(\mathbf{p}) - h_j(\mathbf{p}'))^2 \quad (5)$$

and the kernels:

$$\begin{aligned} \mathcal{K}_{\text{imp}}(\mathbf{p}, \mathbf{p}') &= \frac{g_0^2}{\beta} \delta(\varepsilon_{\mathbf{p}} - \mu) \delta(\varepsilon_{\mathbf{p}'} - \varepsilon_{\mathbf{p}}) \\ \mathcal{K}_{\text{fluct}}^\alpha(\mathbf{p}, \mathbf{p}') &= \frac{g_\alpha^2}{8} \frac{\sinh[\frac{\beta}{2}(\varepsilon_{\mathbf{p}'} - \varepsilon_{\mathbf{p}})]^{-1} \text{Im} \chi_\alpha(\mathbf{p}, \mathbf{p}')}{\cosh[\frac{\beta}{2}(\varepsilon_{\mathbf{p}} - \mu)] \cosh[\frac{\beta}{2}(\varepsilon_{\mathbf{p}'} - \mu)]} \end{aligned} \quad (6)$$

Here, $\alpha = C_a, C_b, S$ refers to the CDW fluctuations around the ordering vectors $\mathbf{Q}_{C,a/b}$ and to the SDW fluctuations around \mathbf{Q}_S . $h_j = \frac{\tau e \beta}{\hbar} \frac{\partial \varepsilon_{\mathbf{k}}}{\partial k_j}$, with $i = x, y$, denotes the deviation of the electronic distribution function n_F from the equilibrium Fermi-Dirac distribution n_F^0 in the presence of an electric field \mathbf{E} , $n_F = n_F^0 - \beta^{-1} (\partial_{\varepsilon} n_F^0) \mathbf{h} \cdot \mathbf{E}$, $\tau^{-1} = g_0^2 / (\pi \nu_F \hbar)$ is the impurity scattering rate and $\rho_0 = \frac{\hbar}{e^2} \frac{2\pi}{\hbar \nu_F \tau} \frac{1}{(v_j^2)_{\mathbf{k}}}$ is the impurity-induced residual resistivity. The electronic dispersion is denoted by $\varepsilon_{\mathbf{p}}$, the CDW and SDW susceptibilities χ_α are given by Eq. (1) and g_0, g_α denote the scattering amplitudes for impurities and fluctuations, respectively.

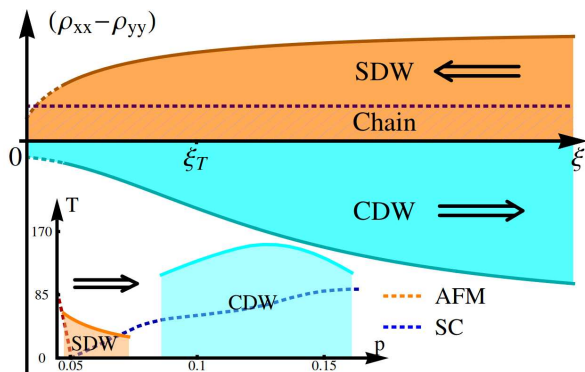


FIG. 4. (color online) Resistivity anisotropy $\rho_a - \rho_b$ due to SDW and CDW fluctuations as function of their correlation lengths $\xi_{S,C}$. The arrows denote how the correlation lengths change as doping increases, as shown schematically in the inset. $\xi_T \propto \sqrt{\Gamma/T}$ is the length scale associated with the thermal excitations of the fluctuations. A constant contribution from the CuO chains in YBCO is indicated as a dashed line.

The collision integrals that determine the resistivity anisotropy (4) are dominated by their behavior near the CDW/SDW hot spots, $\varepsilon_{\mathbf{p}+\mathbf{Q}_\alpha} = \varepsilon_{\mathbf{p}} = 0$, where the susceptibility χ_α is the largest. For the CDW fluctuations, Eq. (1), because the anisotropy is manifested in the correlation length we find that the anisotropy depends only on the Fermi velocity at the hot spots. Introducing the average distance between thermally induced fluctuations $\xi_T = \sqrt{\frac{3\Gamma_C\beta}{2\pi}}$, we obtain in the low-temperature limit $\xi_T \gg \xi_C \gg 1$ the leading-order expression:

$$\left(\frac{\rho_a - \rho_b}{\rho_0}\right)_C \approx \left(\frac{g_C^2 \xi_C^2}{g_0^2 \beta \chi_{0,C}^{-1} \xi_T^2}\right) C_C \eta_C \quad (7)$$

where $\chi_{0,C}^{-1}$ is the CDW energy scale and $C_C < 0$ is a dimensionless positive constant that depends only on the Fermi velocity at the CDW hot spots. Therefore, in YBCO, since $\eta_C > 0$, scattering by charge fluctuations favor $\rho_a < \rho_b$. This can be understood in the following way: since $\eta_C > 0$, fluctuations are stronger around the $\mathbf{Q}_{C,b}$ CDW ordering vector, i.e. $\xi_{C,b} > \xi_{C,a}$. As shown in Fig. 2, at the hot spots connected by $\mathbf{Q}_{C,b}$, the Fermi velocity is almost parallel to the b axis. Thus, electrons moving along the b direction experience enhanced scattering compared to the electrons moving along a , causing $\rho_a < \rho_b$. This argument makes it clear that small deviations in the value of Q_C do not change the result.

As for the SDW fluctuations, the anisotropy does not arise from the ordering vector $\mathbf{Q}_S = (\pi, \pi)$, which is isotropic, but from the form factor. As a result, defining again $\xi_T = \sqrt{\frac{3\Gamma_S\beta}{2\pi}}$ and focusing in the regime

$\xi_T \gg \xi_S \gg 1$, we obtain:

$$\left(\frac{\rho_a - \rho_b}{\rho_0}\right)_S \approx \left(\frac{g_S^2 \ln \xi_S}{g_0^2 \beta \chi_{0,S}^{-1} \xi_T^2}\right) C_S \eta_S \quad (8)$$

In contrast to the CDW case, the dimensionless prefactor C_S depends on the curvature of the Fermi surface and on the derivatives of the Fermi velocity near the hot spots. As a result, C_S may depend on additional details of the Fermi surface, as compared to C_C . We computed it using two different sets of tight-binding parameters [33, 39] and different values of the chemical potential, finding that in general $C_S < 0$. Consequently, since $\eta_S < 0$ in YBCO, scattering by SDW fluctuations yields $\rho_a > \rho_b$. This can be understood as a consequence of the fact that the SDW fluctuations stiffness is smaller along the a axis, since $\eta_S < 0$ in Eq. (1), which enhances the scattering along this direction. Note that, because long-range SDW order is present while long-range CDW order is absent in the underdoped phase diagram, ξ_S can become very large whereas ξ_C remains bounded.

We now contrast our results to the experimental measurements of $\Delta\rho \equiv (\rho_a - \rho_b)/\rho_b$ [1]. In YBCO, the CuO chains, parallel to the b axis, give an intrinsic contribution to the resistivity anisotropy, $\Delta\rho_{\text{chain}} > 0$ (see dashed line in Fig. 4). Thus, the contribution from the CDW/SDW fluctuations add to or subtract from this intrinsic background. As shown in the inset of Fig. 4, anisotropic SDW and CDW fluctuations compete and dominate different regions of the underdoped phase diagram. Starting at $p \approx 0.05$ and increasing p , the anisotropic SDW fluctuations with $\eta_S < 0$ are suppressed as the corresponding transition line disappears near $p \approx 0.08$ [4, 5]. According to our results, $\Delta\rho$ should be positive and should decrease as p increases and ξ_S is suppressed, as shown by the arrow in Fig. 4. This behavior is indeed observed experimentally [1]. CDW fluctuations emerge at $p \approx 0.09$ – initially they are anisotropic, with $\eta_C > 0$, but as $p \approx 0.13$ is approached they become isotropic [5], with $\eta_C \rightarrow 0$. In this regime, we find that the anisotropic CDW fluctuations give $\Delta\rho < 0$. Experimentally, the measured $\Delta\rho$ remains positive in this region, but is the smallest in the phase diagram [1], which could be understood as a consequence of $\Delta\rho < 0$ appearing on the intrinsic $\Delta\rho_{\text{chain}} > 0$ background. To shed light on this issue and disentangle the chains contribution, it would be desirable to perform transport measurements in tetragonal compounds such as $\text{HgBa}_2\text{CuO}_4$ and Nd_2CuO_4 , where CDW fluctuations have also been reported [53, 54]. In this case, application of uniaxial strain [55, 56] would be necessary to select a single nematic domain. Note that for very underdoped YBCO samples, long-range SDW order sets in at very low temperatures [7], giving rise to an anisotropic reconstructed Fermi surface, which promote a non-zero $\Delta\rho$ even in the absence of inelastic scattering at $T = 0$.

In summary, we have shown that the anisotropic charge and spin fluctuations present in YBCO give antagonistic contributions to the resistivity anisotropy in underdoped cuprates. While the SDW fluctuations provide a plausible explanation for the resistivity anisotropy observed experimentally, the contribution of CDW fluctuations seems to be nearly cancelled by the contribution coming from the CuO chains. An open issue is how these anisotropic fluctuations affect other anisotropic transport quantities, such as the thermopower and the Nernst anisotropy [2]. Although a non-zero $\Delta\rho$ is not surprising, since these fluctuations are C_2 symmetric, the fact that the competing fluctuating channels promote different signs for $\Delta\rho$ is unanticipated, opening a promising route to disentangle the contributions from spin and charge degrees of freedom to the formation of the nematic state observed in underdoped cuprates.

We thank M. Chan, A. Chubukov, M. Greven, M. Le Tacon, and J. Schmalian for fruitful discussions. MS acknowledges the support from the Humboldt Foundation. RMF is supported by the U.S. Department of Energy under Award Number DE-SC0012336.

-
- [1] Y. Ando, K. Segawa, S. Komiya, and A. N. Lavrov, *Phys. Rev. Lett.* **88**, 137005 (2002).
- [2] R. Daou, J. Chang, D. LeBoeuf, O. Cyr-Choiniere, F. Laliberte, N. Doiron-Leyraud, B. J. Ramshaw, R. Liang, D. A. Bonn, W. N. Hardy, and L. Taillefer, *Nature* **463**, 519 (2010).
- [3] J. Garcia-Barriocanal, A. Kobrinskii, X. Leng, J. Kinney, B. Yang, S. Snyder, and A. M. Goldman, *Phys. Rev. B* **87**, 024509 (2013).
- [4] M. Hücker, N. B. Christensen, A. T. Holmes, E. Blackburn, E. M. Forgan, R. Liang, D. A. Bonn, W. N. Hardy, O. Gutowski, M. v. Zimmermann, S. M. Hayden, and J. Chang, *Phys. Rev. B* **90**, 054514 (2014).
- [5] S. Blanco-Canosa, A. Frano, E. Schierle, J. Porras, T. Loew, M. Minola, M. Bluschke, E. Weschke, B. Keimer, and M. Le Tacon, *Phys. Rev. B* **90**, 054513 (2014).
- [6] V. Hinkov, D. Haug, B. Fauqué, P. Bourges, Y. Sidis, A. Ivanov, C. Bernhard, C. T. Lin, and B. Keimer, *Science* **319**, 597 (2008).
- [7] D. Haug, V. Hinkov, Y. Sidis, P. Bourges, N. B. Christensen, A. Ivanov, T. Keller, C. T. Lin, and B. Keimer, *New Journal of Physics* **12**, 105006 (2010).
- [8] M. J. Lawler, K. Fujita, L. Jhinhwan, A. R. Schmidt, Y. Kohsaka, K. C. Koo, H. Eisaki, S. Uchida, J. C. Davis, J. P. Sethna, and K. Eun-Ah, *Nature* **466**, 347 (2010).
- [9] S. A. Kivelson, E. Fradkin, and V. J. Emery, *Nature* **393**, 550 (1998).
- [10] S. A. Kivelson, I. P. Bindloss, E. Fradkin, V. Oganessian, J. M. Tranquada, A. Kapitulnik, and C. Howald, *Rev. Mod. Phys.* **75**, 1201 (2003).
- [11] M. Vojta, *Advances in Physics* **58**, 699 (2009).
- [12] E. Fradkin, S. A. Kivelson, M. J. Lawler, J. P. Eisenstein, and A. P. Mackenzie, *Annual Review of Condensed Matter Physics* **1**, 153 (2010).
- [13] Y. Li, V. Baledent, N. Barisic, Y. Cho, B. Fauque, Y. Sidis, G. Yu, X. Zhao, P. Bourges, and M. Greven, *Nature* **455**, 372 (2008).
- [14] A. Shekhter, B. J. Ramshaw, R. Liang, W. N. Hardy, D. A. Bonn, F. F. Balakirev, R. D. McDonald, J. B. Betts, S. C. Riggs, and A. Migliori, *Nature* **498**, 75 (2013).
- [15] J. Zaanen and O. Gunnarsson, *Phys. Rev. B* **40**, 7391 (1989).
- [16] K. Machida, *Physica C: Superconductivity* **158**, 192 (1989).
- [17] R. M. Fernandes, J. Schmalian, and H. Westfahl, *Phys. Rev. B* **78**, 184201 (2008).
- [18] E. Blackburn, J. Chang, M. Hücker, A. T. Holmes, N. B. Christensen, R. Liang, D. A. Bonn, W. N. Hardy, U. Rütt, O. Gutowski, M. v. Zimmermann, E. M. Forgan, and S. M. Hayden, *Phys. Rev. Lett.* **110**, 137004 (2013).
- [19] S. Blanco-Canosa, A. Frano, T. Loew, Y. Lu, J. Porras, G. Ghiringhelli, M. Minola, C. Mazzoli, L. Braicovich, E. Schierle, E. Weschke, M. Le Tacon, and B. Keimer, *Phys. Rev. Lett.* **110**, 187001 (2013).
- [20] T. Wu, H. Mayaffre, S. Kramer, M. Horvatic, C. Berthier, W. N. Hardy, R. Liang, D. A. Bonn, and M.-H. Julien, *Nature* **477**, 191 (2011).
- [21] T. Wu, H. Mayaffre, S. Krämer, M. Horvatic, C. Berthier, W. Hardy, R. Liang, D. Bonn, and M.-H. Julien, *Nature Communications* **6** (2015), doi:10.1038/ncomms7438.
- [22] V. Oganessian, S. A. Kivelson, and E. Fradkin, *Phys. Rev. B* **64**, 195109 (2001).
- [23] S. A. Kivelson, E. Fradkin, and T. H. Geballe, *Phys. Rev. B* **69**, 144505 (2004).
- [24] C. Fang, H. Yao, W.-F. Tsai, J. P. Hu, and S. A. Kivelson, *Phys. Rev. B* **77**, 224509 (2008).
- [25] K. Sun, M. J. Lawler, and E.-A. Kim, *Phys. Rev. Lett.* **104**, 106405 (2010).
- [26] M. H. Fischer and E.-A. Kim, *Phys. Rev. B* **84**, 144502 (2011).
- [27] L. Nie, G. Tarjus, and S. A. Kivelson, *Proceedings of the National Academy of Sciences* **111**, 7980 (2014).
- [28] S. Bulut, W. A. Atkinson, and A. P. Kampf, *Phys. Rev. B* **88**, 155132 (2013).
- [29] Y. Wang and A. Chubukov, *Phys. Rev. B* **90**, 035149 (2014).
- [30] E. Fradkin, S. A. Kivelson, and J. M. Tranquada, *arxiv:1407.4480* (2014).
- [31] M. A. Metlitski and S. Sachdev, *Phys. Rev. B* **82**, 075128 (2010).
- [32] K. B. Efetov, H. Meier, and C. Pepin, *Nat Phys* **9**, 442 (2013).
- [33] S. Sachdev and R. La Placa, *Phys. Rev. Lett.* **111**, 027202 (2013).
- [34] A. Allais, J. Bauer, and S. Sachdev, *Phys. Rev. B* **90**, 155114 (2014).
- [35] R. Comin, A. Frano, M. M. Yee, Y. Yoshida, H. Eisaki, E. Schierle, E. Weschke, R. Sutarto, F. He, A. Soumyanarayanan, Y. He, M. Le Tacon, I. S. Elfimov, J. E. Hoffman, G. A. Sawatzky, B. Keimer, and A. Damascelli, *Science* **343**, 390 (2014).
- [36] A. Melikyan and M. R. Norman, *Phys. Rev. B* **89**, 024507 (2014).
- [37] A. M. Tsvelik and A. V. Chubukov, *Physical Review B* **89**, 184515 (2014).

- [38] W. A. Atkinson, Phys. Rev. B **59**, 3377 (1999).
- [39] T. Das, Phys. Rev. B **86**, 064527 (2012).
- [40] R. M. Fernandes, A. V. Chubukov, and J. Schmalian, Nature Physics **10**, 97 (2014).
- [41] See Supplemental Material [url], which includes Refs.[33, 38, 39, 42, 43, 57].
- [42] A. Rosch, Phys. Rev. Lett. **82**, 4280 (1999).
- [43] R. M. Fernandes, E. Abrahams, and J. Schmalian, Phys. Rev. Lett. **107**, 217002 (2011).
- [44] J. M. Buhmann, M. Ossadnik, T. M. Rice, and M. Sigrist, Phys. Rev. B **87**, 035129 (2013).
- [45] N. Barišić, M. K. Chan, Y. Li, G. Yu, X. Zhao, M. Dressel, A. Smontara, and M. Greven, Proceedings of the National Academy of Sciences **110**, 12235 (2013).
- [46] M. K. Chan, M. J. Veit, C. J. Dorow, Y. Ge, Y. Li, W. Tabis, Y. Tang, X. Zhao, N. Barišić, and M. Greven, Phys. Rev. Lett. **113**, 177005 (2014).
- [47] S. I. Mirzaei, D. Stricker, J. N. Hancock, C. Berthod, A. Georges, E. van Heumen, M. K. Chan, X. Zhao, Y. Li, M. Greven, N. Barišić, and D. van der Marel, Proceedings of the National Academy of Sciences **110**, 5774 (2013).
- [48] M. J. Lawler, D. G. Barci, V. Fernández, E. Fradkin, and L. Oxman, Phys. Rev. B **73**, 085101 (2006).
- [49] M. J. Lawler and E. Fradkin, Phys. Rev. B **75**, 033304 (2007).
- [50] J. Nilsson and A. H. Castro Neto, Phys. Rev. B **72**, 195104 (2005).
- [51] E. W. Carlson, K. A. Dahmen, E. Fradkin, and S. A. Kivelson, Physical review letters **96**, 097003 (2006).
- [52] B. M. Andersen, S. Graser, and P. J. Hirschfeld, EPL (Europhysics Letters) **97**, 47002 (2012).
- [53] E. H. Neto, R. Comin, F. He, R. Sutarto, Y. Jiang, R. L. Greene, G. A. Sawatzky, and A. Damascelli, arxiv:1410.2253 (2014).
- [54] W. Tabis, Y. Li, M. Le Tacon, L. Braicovich, A. Kreyssig, M. Minola, G. Dellea, E. Weschke, M. J. Veit, M. Ramazanoglu, A. I. Goldman, T. Schmitt, G. Ghiringhelli, N. Barišić, M. K. Chan, C. J. Dorow, G. Yu, X. Zhao, B. Keimer, and M. Greven, arxiv:1404.7658 (2014).
- [55] J.-H. Chu, J. G. Analytis, K. De Greve, P. L. McMahon, Z. Islam, Y. Yamamoto, and I. R. Fisher, Science **329**, 824 (2010).
- [56] M. A. Tanatar, E. C. Blomberg, A. Kreyssig, M. G. Kim, N. Ni, A. Thaler, S. L. Bud'ko, P. C. Canfield, A. I. Goldman, I. I. Mazin, and R. Prozorov, Phys. Rev. B **81**, 184508 (2010).
- [57] J. Ziman, *Electrons and Phonons: The Theory of Transport Phenomena in Solids*, Oxford Classic Texts in the Physical Sciences (OUP Oxford, 2001).
-

I. SUPPLEMENTARY MATERIAL

A. Anisotropic fluctuations and the coupling to the chains in YBCO

As explained in the main text, the changes in the susceptibility caused by the coupling to the CuO chains present in the YBCO compounds can be evaluated via the polarization operator:

$$\tilde{\chi}_\alpha^{-1}(\mathbf{q}) - [\chi_\alpha^{-1}(\mathbf{q})]_{\eta_C=\eta_S=0} = -\delta\Pi(\mathbf{q}). \quad (9)$$

with $\alpha = C, S$ and χ_α^{-1} given by Eq. (1) of the main text. Here we are interested only in the anisotropic properties: $\delta\Pi(\mathbf{q}) = \Pi(\mathbf{q}) - \Pi_{\text{no-chain}}(\mathbf{q})$, which by definition must arise from the coupling to the CuO chains, since the electronic dispersion due to the CuO₂ planes is tetragonally symmetric. We emphasize that, in our approach, the role played by the chains is to simply induce a conjugate field that selects a particular nematic domain, and not to cause the nematic instability in the first place. The polarization operator is given by the standard expression:

$$\Pi(\mathbf{q}) = \beta^{-1} \sum_{\omega_n} \int \frac{d^2p}{(2\pi)^2} \text{Tr} [\mathcal{G}(i\omega_n, \mathbf{p}) \mathcal{G}(i\omega_n, \mathbf{p} - \mathbf{q})], \quad (10)$$

where \mathcal{G} denotes the non-interacting matrix Green's function of the multi-band system consisting of the CuO₂ plane and the CuO chain. Even though YBCO has two CuO₂ planes per unit cell, the main results are captured by a simpler two-band model consisting of a single plane and a single chain, defined via the spinor $\Psi_{\mathbf{k}\sigma}^\dagger = \left(d_{p,\mathbf{k}\sigma}^\dagger \quad d_{c,\mathbf{k}\sigma}^\dagger \right)$ where p, c denote plane or chain operators, respectively. The corresponding non-interacting Hamiltonian is therefore given by $H^{(2)} = \sum_{\mathbf{k}\sigma} \Psi_{\mathbf{k}\sigma}^\dagger \mathcal{H}_{\mathbf{k}}^{(2)} \Psi_{\mathbf{k}\sigma}$ with the matrix:

$$\mathcal{H}_{\mathbf{k}}^{(2)} = \begin{pmatrix} \epsilon_p(\mathbf{k}) & t_{cp} \\ t_{cp} & \epsilon_c(\mathbf{k}) \end{pmatrix} \quad (11)$$

Here we defined the tight-binding dispersions of the plane and of the chain [33, 39]:

$$\begin{aligned} \epsilon_p(\mathbf{k}) &= -2t(\cos k_x + \cos k_y) - 4t' \cos k_x \cos k_y - 2t''(\cos 2k_x + \cos 2k_y) - \mu_p, \\ \epsilon_c(\mathbf{k}) &= -2t_c \cos k_y - \mu_c. \end{aligned} \quad (12)$$

and the plane-chain hopping parameter t_{cp} . The main effects of the coupling to the chain can be understood analytically by considering the limit $t_{cp} \ll |\mu_c|$. In this case, the effective plane dispersion becomes:

$$\tilde{\epsilon}_p(\mathbf{k}) = -2\tilde{t}(\cos k_x + \cos k_y) + 2\delta(\cos k_x - \cos k_y) - 4\tilde{t}' \cos k_x \cos k_y - 2\tilde{t}''(\cos 2k_x + \cos 2k_y) - \tilde{\mu}_p \quad (13)$$

with the modified tight-binding parameters: $\tilde{t} = t - \left(\frac{t_{cp}}{\mu_c}\right)^2 (t - t_c)$, $\delta = \left(\frac{t_{cp}}{\mu_c}\right)^2 t_c$ and $\tilde{\mu}_p = \mu_p + \frac{2t_{cp}^2}{|\mu_c|}$. The main change in the dispersion is the appearance of the anisotropic term with coefficient $\delta > 0$. Since $\tilde{t} > 0$, this term effectively reduces the Fermi-momentum along the k_y direction. As a result, the Fermi surface is squeezed (relative to the (π, π) point), becoming more elongated along the k_x axis than along the k_y axis, as shown in Figure 5.

The impact of these changes on the polarization operator can be understood in a straightforward way. The squeezing of the Fermi surface promotes extended and relatively flat segments displaced along the k_y direction. Because these flat segments provide an enhanced contribution to the density response, the CDW fluctuations near the ordering vector $\mathbf{Q}_{C,b}$ are favored compared to the fluctuations centered at $\mathbf{Q}_{C,a}$. Similarly, the SDW fluctuations, centered at $\mathbf{Q}_S = (\pi, \pi)$, become stiffer along the k_y direction, as compared to the k_x direction.

For the numerical evaluation presented in Figure 2 of the main text, we used the band structure parameters of Ref. [39]. In particular, to make the chain effect more visible, we considered a larger value of the chain-plane coupling t_{cp} than the one in Ref. [39]. The parameters used were, in eV, $(t, t_1, t_2, \mu_p, t_c, \mu_c, t_{cp}) = (0.38, 0.0684, 0.095, 0, 0.25, -0.87, -0.075)$. As mentioned above, in YBCO two planes are actually coupled to the same CuO chain in each unit cell. A more precise model therefore starts with the three-component spinor $\Psi_{\mathbf{k}\sigma}^\dagger = \left(d_{p_1,\mathbf{k}\sigma}^\dagger \quad d_{p_2,\mathbf{k}\sigma}^\dagger \quad d_{c,\mathbf{k}\sigma}^\dagger \right)$ and the Hamiltonian $H^{(3)} = \sum_{\mathbf{k}\sigma} \Psi_{\mathbf{k}\sigma}^\dagger \mathcal{H}_{\mathbf{k}}^{(3)} \Psi_{\mathbf{k}\sigma}$ with [38]:

$$\mathcal{H}_{\mathbf{k}}^{(3)} = \begin{pmatrix} \epsilon_p(\mathbf{k}) & t_{pp} & t_{cp} \\ \epsilon_{pp} & \epsilon_p(\mathbf{k}) & t_{cp} \\ t_{cp} & t_{cp} & \epsilon_c(\mathbf{k}) \end{pmatrix} \quad (14)$$

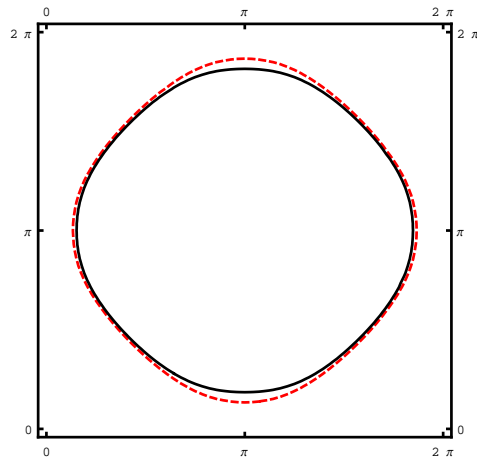


FIG. 5. Distortion of the Fermi surface due to the coupling between the plane and the CuO chain. For clarity, we increase the value of t_{cp} to 0.1, we shift the origin of the Brillouin zone to (π, π) and display both the distorted (solid line) and undistorted (dashed line) Fermi surfaces.

The non-zero inter-plane hopping $t_{pp} > 0$ gives rise to bonding and anti-bonding bands, i.e. $\epsilon_p^{(\pm)}(\mathbf{k}) = \epsilon_p(\mathbf{k}) \pm t_{pp}$. Once the coupling to the chains is included, only the anti-bonding band $\epsilon_p^{(+)}(\mathbf{k})$ is in fact affected by t_{cp} and becomes anisotropic, similarly to Eq. (13). Therefore, as long as the plane-chain coupling is not too large compared to the inter-plane hopping, $|t_{cp}| \ll t_{pp}$, we find that the anisotropy in the polarization operator is the same as in the case of a single plane coupled to the chains, since the anisotropy of the Fermi surface is the same as in Eq. (13).

B. Anisotropic Transport: Boltzmann equation formalism

1. Fermi surface parametrization

To solve the Boltzmann equation, it is convenient to have a suitable parametrization of the Fermi surface of the usual cuprate tight-binding models [33, 39]. Since we are interested in the hole-underdoped regime, it is convenient to shift the center of the Brillouin zone to (π, π) , around which the Fermi surface is closed. In particular, it can be parametrized by:

$$\mathbf{p}_F(\phi) = \bar{p}_F f(\phi) \begin{pmatrix} \cos \phi \\ \sin \phi \end{pmatrix} \quad \text{while } \epsilon_p(\mathbf{p}_F(\phi)) - \mu = 0, \quad (15)$$

where f is a dimensionless function encoding the form of the Fermi surface and \bar{p}_F is a radial coordinate proportional to the Fermi momentum scale. Here, ϕ is the angle measured relative to the k_x axis. Away from the Fermi level, the momentum is parametrized by $\mathbf{p}(\bar{p}, \phi) = \mathbf{p}_F(\phi) \bar{p}/\bar{p}_F$. Thus, near the Fermi level, we can expand the dispersion as:

$$\epsilon_p(\mathbf{p}(\bar{p}, \phi)) - \mu \approx \mathbf{v}_F(\phi) \cdot \mathbf{p}_F(\phi) \left(\frac{\bar{p}}{\bar{p}_F} - 1 \right) \quad (16)$$

allowing us to express the radial component in terms of an energy variable ϵ , $\bar{p}/\bar{p}_F = 1 + \epsilon/(\mathbf{v}_F(\phi) \cdot \mathbf{p}_F(\phi))$. For convenience, we identify the angle-dependent energy scale $\mathbf{v}_F(\phi) \cdot \mathbf{p}_F(\phi) = \epsilon_F(\phi)$. To evaluate the sums over momentum that appear in the Boltzmann equation solution, we define the angle-dependent density of states $N_\phi = \mathbf{p}_F^2(\phi)/|\epsilon_F(\phi)|$, such that the total density of states ν_F is given by $\nu_F = \int \frac{d\phi}{2\pi} N_\phi$. Then, for an arbitrary function K strongly peaked at the Fermi surface we have:

$$\int \frac{d^2 p}{(2\pi\hbar)^2} K(\epsilon_p(\mathbf{p}) - \mu, \mathbf{p}) \approx \nu_F \left\langle \int \frac{d\epsilon}{2\pi} K(\epsilon, \mathbf{p}_F(\phi)) \right\rangle_\phi. \quad (17)$$

where we introduced the notation:

$$\nu_F \langle F(\phi) \rangle_\phi = \int \frac{d\phi}{2\pi} N_\phi F(\phi). \quad (18)$$

2. *Functional Approach to the Boltzmann equation*

The Boltzmann equation for scattering by impurities and fluctuations is given by:

$$\left(\frac{\partial}{\partial t} + \mathbf{v} \cdot \nabla_{\mathbf{r}} + e\mathbf{E} \cdot \mathbf{v} \frac{\partial}{\partial \epsilon} \right) n_F = -\mathcal{I}_{\text{imp}}[n_F] - \sum_{\alpha} \mathcal{I}_{\text{fluct}}^{\alpha}[n_F], \quad (19)$$

with $\alpha = C_a, C_b, S$. In linear response, we consider weak perturbations around equilibrium: $n_F = n_F^0 - \frac{\partial n_F^0}{\partial \epsilon} \beta^{-1} h$. Keeping only the driving field, the linearized Boltzmann equation becomes:

$$e\mathbf{E} \cdot \mathbf{v} \frac{\partial n_F^0}{\partial \epsilon} = -\delta\mathcal{I}_{\text{imp}}[h] - \sum_{\alpha} \delta\mathcal{I}_{\text{fluct}}^{\alpha}[h]. \quad (20)$$

Instead of solving the integral equation above, the solution of the Boltzmann equation can be obtained by minimization of the functional [42, 43, 57]:

$$F[h] = -D[h] + I_{\text{imp}}[h] + \sum_{\alpha} I_{\text{fluct}}^{\alpha}[h] \quad (21)$$

Because $\epsilon_F(\phi) \gg T$, we have $\frac{\partial n_F^0}{\partial \epsilon} \approx -\delta(\epsilon_F - \mu)$, implying that the deviations from equilibrium depend only on the angle parametrizing the Fermi-surface, $h(\phi)$. Defining the unit vector $\mathbf{E}_i = E\mathbf{e}_i$, the functionals can be expressed as:

$$\begin{aligned} D_i[h_j] &= \frac{(eE)\nu_F}{2\pi} \langle \mathbf{e}_i \cdot \mathbf{v}_F(\phi) h_j(\phi) \rangle_{\phi}, \\ I_{\text{imp}}[h_j] &= \frac{g_0^2}{2(2\pi)^2 \hbar \beta} \langle (h_j(\phi) - h_j(\phi'))^2 \rangle_{\phi, \phi'}, \\ I_{\text{fluct}}^{\alpha}[h_j] &= \frac{g_{\alpha}^2}{16\hbar} \left\langle \int \frac{d\epsilon}{2\pi} \int \frac{d\epsilon'}{2\pi} \frac{\text{Im} \chi_{\alpha}(\epsilon' - \epsilon; \phi, \phi') (h_j(\phi) - h_j(\phi'))^2}{\cosh[\frac{\beta}{2}\epsilon] \cosh[\frac{\beta}{2}\epsilon'] \sinh[\frac{\beta}{2}(\epsilon' - \epsilon)]} \right\rangle_{\phi, \phi'} \end{aligned} \quad (22)$$

We are interested in the regime where the elastic impurity scattering is dominant. In this regime, the deviation from equilibrium is given by: $h_i = \tau \beta e E \mathbf{e}_i \cdot \mathbf{v}$, where τ^{-1} is the impurity scattering rate, yielding $D_i[\beta e \mathbf{E}_j \cdot \mathbf{v}] = (eE)^2 \bar{D}_{ij}$, $I_{\text{imp}}[\beta e \mathbf{E}_j \cdot \mathbf{v}] = (eE)^2 \bar{I}_{\text{eff},j}$ and $I_{\text{fluct}}^i[\beta e \mathbf{E}_j \cdot \mathbf{v}] = (eE)^2 \bar{I}_{\text{fluct}}^{\alpha}$. The residual resistivity is therefore given by:

$$\rho_0^{-1} = \frac{1}{2} \left(\frac{D_x[h_x]}{\beta E^2} + \frac{D_y[h_y]}{\beta E^2} \right) = \frac{e^2 \hbar^2 \nu_F^2}{\hbar} \frac{2g_0^2}{2g_0^2} \langle v_j^2 \rangle_{\phi} = \frac{e^2 \hbar \nu_F \tau}{\hbar} \frac{2\pi}{2\pi} \langle v_j^2 \rangle_{\phi} \quad (23)$$

Note that, in principle, since we are interested in the resistivity anisotropy, we could also include the isotropic contribution from the fluctuations to the definition of an effective isotropic scattering rate τ^{-1} . The anisotropic resistivity becomes:

$$\rho_a - \rho_b = \rho_0 \frac{\sum_{\alpha} \delta \bar{I}_{\text{fluct}}^{\alpha}}{\bar{I}_{\text{imp}}} \quad (24)$$

with:

$$\bar{I}_{\text{imp}} = \frac{g_0^2 \beta}{(2\pi)^2 \hbar} \langle \mathbf{v}_F^2(\phi) \rangle_{\phi} \quad (25)$$

$$\delta \bar{I}_{\text{fluct}}^{\alpha} = \frac{g_{\alpha}^2 \chi_{0,\alpha}}{8\pi \hbar} J_{\text{fluct}}^{\alpha} \quad (26)$$

with $J_{\text{fluct}}^{\alpha}$ given by:

$$J_{\text{fluct}}^{\alpha} = \frac{\pi \beta^2}{2\nu_F^2 \chi_{0,\alpha}} \int \frac{d^2 p'}{(2\pi \hbar)^2} \int \frac{d^2 p}{(2\pi \hbar)^2} \frac{(\mathbf{e}_x \cdot \mathbf{v} - \mathbf{e}_x \cdot \mathbf{v}')^2 - (\mathbf{e}_y \cdot \mathbf{v} - \mathbf{e}_y \cdot \mathbf{v}')^2}{\cosh[\frac{\beta}{2}(\epsilon_p - \mu)] \cosh[\frac{\beta}{2}(\epsilon_{p'} - \mu)] \sinh[\frac{\beta}{2}(\epsilon_{p'} - \epsilon_p)]} \text{Im} \chi_{\alpha}(\epsilon' - \epsilon; \phi, \phi') \quad (27)$$

Here, we defined the energy scale $\chi_{0,\alpha}^{-1}$ that characterizes the fluctuation spectrum. The resistivity anisotropy is then given by:

$$\rho_a - \rho_b = \rho_0 \sum_{\alpha} \frac{\pi g_{\alpha}^2}{2 g_0^2} \frac{\chi_{0,\alpha}}{\beta} \frac{J_{\text{fluct}}^{\alpha}}{\langle \mathbf{v}_F^2(\phi) \rangle_{\phi}} \quad (28)$$

Note that, in this Boltzmann equation approach, we neglect the renormalization of the Fermi velocity by the fluctuations as well as weak-localization corrections. These contributions are only important at very low temperatures, in the regime $T \ll \tau^{-1}$, which is not relevant for our analysis.

C. evaluation of the resistivity anisotropy

1. Hot spots contribution

In this section we present the numerical and analytical evaluation of $J_{\text{fluct}}^{\alpha}$ defined in Eq. (27), obtaining consequently the resistivity anisotropy (28). First, we define the general form of the susceptibility that can describe either of the CDW fluctuations (around $\mathbf{Q}_{C,a}$ and $\mathbf{Q}_{C,b}$) or the SDW fluctuations (around \mathbf{Q}_S):

$$\frac{\chi_{\alpha}^{-1}(\mathbf{q}, \omega)}{\chi_0^{-1}} = \left[\xi_{\alpha}^{-2} + (1 + \eta_{\alpha}) (q_x - Q_{\alpha,x})^2 + (1 - \eta_{\alpha}) (q_y - Q_{\alpha,y})^2 \right] - i \frac{\omega}{\Gamma_{\alpha}} \equiv \tilde{\omega}_{\alpha,q} - i \frac{\omega}{\Gamma_{\alpha}}. \quad (29)$$

where all lengths are measured relative to the lattice parameter a . Hereafter, for simplicity of notation, we drop the subscript α . Defining the length scale $\xi_T^2 = 3\Gamma\beta/(2\pi)$ measuring the mean distance between thermally excited fluctuations, and using the following integral evaluation/approximation:

$$\int d\epsilon \frac{1}{\cosh[\frac{\beta}{2}(\epsilon_p - \mu)] \cosh[\frac{\beta}{2}(\epsilon_p + \omega - \mu)]} = \frac{2\omega}{\sinh[\omega\beta/2]} \quad (30)$$

$$\int d\omega \frac{\omega}{\sinh[\omega\beta/2]^2} \frac{\omega \chi_0 \Gamma}{\Gamma^2 \tilde{\omega}_q^2 + \omega^2} \approx \frac{4\chi_0}{3\Gamma\beta^3} \frac{2\pi^2}{\tilde{\omega}_q(\tilde{\omega}_q + \frac{2\pi}{3\Gamma\beta})}. \quad (31)$$

we obtain:

$$J_{\text{fluct}}^{\alpha} = \xi_T^{-2} \left\langle \frac{(\mathbf{e}_x \cdot \mathbf{v} - \mathbf{e}_x \cdot \mathbf{v}')^2 - (\mathbf{e}_y \cdot \mathbf{v} - \mathbf{e}_y \cdot \mathbf{v}')^2}{\tilde{\omega}_q(\phi, \phi') [\tilde{\omega}_q(\phi, \phi') + \xi_T^{-2}]} \right\rangle_{\phi, \phi'} \quad (32)$$

Clearly, the main contribution to the integral above comes from the hot spots, which can be parametrized by two angles ϕ_1 and ϕ_2 defined via $\mathbf{Q} = \mathbf{q} = \mathbf{p}_F(\phi_1) - \mathbf{p}_F(\phi_2)$. In the following, we compute Eq. (32) both numerically, using the tight-binding dispersion of Ref. [39], and analytically via an expansion near the hot spots. We consider the CDW and SDW cases separately, for convenience.

2. CDW fluctuations

The CDW hot spots are connected by the ordering vectors $\mathbf{Q}_{C,a} = Q_c \hat{\mathbf{x}}$ and $\mathbf{Q}_{C,b} = Q_c \hat{\mathbf{y}}$. In the coordinate system centered at the (π, π) point of the Brillouin zone, pairs of hot spots connected by $\mathbf{Q}_{C,a}$ correspond to $\phi_1, \phi_2 = \pi - \phi_1$, whereas the pairs of hot spots connected by $\mathbf{Q}_{C,b}$ correspond to $\phi_1, \phi_2 = -\phi_1$. Expansion around these angles, for the hot spots connected by $\mathbf{Q}_{C,a}$, gives:

$$q_y - Q_{a,y} \approx (\delta\phi_1 + \delta\phi_2) \left[\frac{\partial p_y}{\partial \phi_1} + \frac{1}{2} \frac{\partial^2 p_y}{\partial \phi_1^2} (\delta\phi_1 - \delta\phi_2) \right] \quad (33)$$

$$q_x - Q_{a,x} \approx (\delta\phi_1 - \delta\phi_2) \left[\frac{\partial p_x}{\partial \phi_1} + \frac{1}{2} \frac{\partial^2 p_x}{\partial \phi_1^2} (\delta\phi_1 + \delta\phi_2) \right] \quad (34)$$

For the hot spots connected by $\mathbf{Q}_{C,b}$, the two functional forms of the right-hand sides are exchanged. As a result, we obtain:

$$\tilde{\omega}_q = \xi_{C,j}^2 + \left(\frac{\partial p_x}{\partial \phi_1} \right)^2 r^2 + \left(\frac{\partial p_y}{\partial \phi_1} \right)^2 s^2 \quad (35)$$

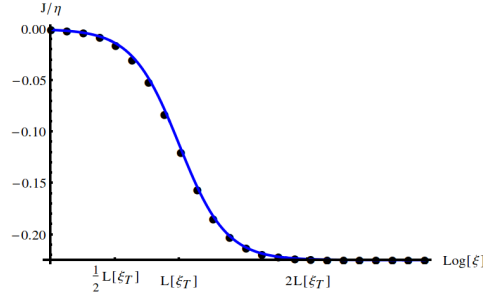


FIG. 6. Comparison of the analytic approximation to J_{fluct}^C given by Eq. (36) (solid blue line) with the numerical evaluation of the corresponding integral in Eq. (32) (black dots). For convenience, we defined $L(\xi_T) \equiv \ln(\xi_T)$.

where r and s are defined as $r = \delta\phi_1 - \delta\phi_2$ and $s = \delta\phi_1 + \delta\phi_2$ for $\mathbf{Q}_{C,a}$ (both are exchanged for $\mathbf{Q}_{C,b}$). Evaluation of the integral in Eq. (32), with $J_{\text{fluct}}^\alpha = J_{\text{fluct}}^{\alpha,x} + J_{\text{fluct}}^{\alpha,y}$, gives:

$$J_{\text{fluct}}^{C,j} = \frac{1}{4\pi} \left(\frac{N_{\phi_1}}{\nu_F} \right)^2 \frac{\ln \left[1 + \left(\frac{\xi_{C,j}}{\xi_T} \right)^2 \right]}{\left| \frac{\partial p_x}{\partial \phi_1} \frac{\partial p_y}{\partial \phi_1} \right|} \begin{cases} 4v_x^2(\phi_1^x) & \text{for } \mathbf{Q}_{C,a} \\ -4v_y^2(\phi_1^y) & \text{for } \mathbf{Q}_{C,b} \end{cases}$$

where we used $N_{\phi_1} = N_{\phi_2}$. Because $v_y^2(\phi_1^y = \phi_1^x + \frac{\pi}{2}) = v_x^2(\phi_1^x)$, the only term that gives rise to an anisotropic resistivity is $\xi_{C,a} \neq \xi_{C,b}$. Expanding to leading order in the nematic order parameter $\eta_C = (\xi_{C,a}^{-2} - \xi_{C,b}^{-2}) / 2\xi_C^{-2}$ yields:

$$J_{\text{fluct}}^C \approx \left[\frac{2 \langle \mathbf{v}_F^2(\phi) \rangle_\phi}{\pi} \right] \frac{C_C \eta_C}{\left(\frac{\xi_T}{\xi_C} \right)^2 + 1} \quad (36)$$

with the negative geometrical pre-factor:

$$C_C = - \left(\frac{N_{\phi_1}}{\nu_F} \right)^2 \frac{v_x^2(\phi_1^x)}{2 \langle \mathbf{v}_F^2(\phi) \rangle_\phi \left| \frac{\partial p_x}{\partial \phi_1} \frac{\partial p_y}{\partial \phi_1} \right|} \quad (37)$$

In order to estimate the precision of the asymptotic result obtained above we compared it with the corresponding numerical evaluation of J_{fluct}^C in Fig. 6 using the tight-binding dispersion of Ref. [39] with $\mu = 0.1$. We checked that the agreement is robust for changes in the chemical potential and also for other tight-binding dispersions, such as that used in Ref. [33].

3. SDW fluctuations

The contribution from the SDW fluctuations are more involved due to the higher symmetry of the fluctuations. The hot spots, connected by the ordering vector $\mathbf{Q}_S = (\pi, \pi)$, correspond to the angles $\phi_1, \phi_2 = \frac{3\pi}{2} - \phi_1$. Expansion around these angles gives:

$$q_x - Q_x \approx \frac{\partial p_x}{\partial \phi_1} \delta\phi_1 - \frac{\partial p_y}{\partial \phi_1} \delta\phi_2 + \frac{1}{2} \frac{\partial^2 p_x}{\partial \phi_1^2} \delta\phi_1^2 + \frac{1}{2} \frac{\partial^2 p_y}{\partial \phi_1^2} \delta\phi_2^2 \quad (38)$$

$$q_y - Q_y \approx \frac{\partial p_y}{\partial \phi_1} \delta\phi_1 - \frac{\partial p_x}{\partial \phi_1} \delta\phi_2 + \frac{1}{2} \frac{\partial^2 p_y}{\partial \phi_1^2} \delta\phi_1^2 + \frac{1}{2} \frac{\partial^2 p_x}{\partial \phi_1^2} \delta\phi_2^2 \quad (39)$$

Unlike the CDW case, an expansion only in the denominator of Eq. (32) is however not enough, because the anisotropy comes from the momentum-dependent part of the susceptibility. Therefore, we expand also the angle-dependent DOS:

$$N_\phi N_{\phi'} \approx N_{\phi_1}^2 \left[1 + (\delta\phi_1 - \delta\phi_2) \frac{\partial}{\partial\phi} \ln(N_\phi) \right] = N_{\phi_1}^2 [1 + \mu_{\phi_1} (\delta\phi_1 - \delta\phi_2)] \quad (40)$$

as well as the velocity combination:

$$(v_x(\phi_1 + \delta\phi_1) - v_x(\phi_2 + \delta\phi_2))^2 - (v_y(\phi_1 + \delta\phi_1) - v_y(\phi_2 + \delta\phi_2))^2 \approx (\delta\phi_1 + \delta\phi_2) [A_1 + A_2 (\delta\phi_1 - \delta\phi_2)] \quad (41)$$

with

$$A_1 = 2(v_x(\phi_1) + v_y(\phi_1)) \left(\frac{\partial v_x}{\partial\phi_1} - \frac{\partial v_y}{\partial\phi_1} \right) \quad (42)$$

$$A_2 = \left[\left(\frac{\partial v_x}{\partial\phi_1} \right)^2 - \left(\frac{\partial v_y}{\partial\phi_1} \right)^2 + (v_x(\phi_1) + v_y(\phi_1)) \left(\frac{\partial^2 v_x}{\partial\phi_1^2} - \frac{\partial^2 v_y}{\partial\phi_1^2} \right) \right]. \quad (43)$$

It is straightforward to recognize that the transformation $(\delta\phi_1, \delta\phi_2) \leftrightarrow -(\delta\phi_2, \delta\phi_1)$ is equivalent to $(q_y - Q_y) \leftrightarrow (q_x - Q_x)$. Since this transformation does not alter the measure and merely changes the global sign of the velocity part we split $\tilde{\omega}_q$ into odd (L) and even (K) parts with respect to the transformation above:

$$\tilde{\omega}_q = \xi_S^{-2} + K_1 + K_2 + \eta_S(L_1 + L_2) \quad (44)$$

with the leading order (K_1, L_1) and next-to-leading order (K_2, L_2) contributions:

$$K_1 = \frac{1}{2} \left(\frac{\partial p_x}{\partial\phi_1} + \frac{\partial p_y}{\partial\phi_1} \right)^2 (\delta\phi_1 - \delta\phi_2)^2 + \frac{1}{2} \left(\frac{\partial p_x}{\partial\phi_1} - \frac{\partial p_y}{\partial\phi_1} \right)^2 (\delta\phi_1 + \delta\phi_2)^2 \quad (45)$$

$$K_2 = \left(\frac{\partial p_x}{\partial\phi_1} \frac{\partial^2 p_x}{\partial\phi_1^2} + \frac{\partial p_y}{\partial\phi_1} \frac{\partial^2 p_y}{\partial\phi_1^2} \right) (\delta\phi_1^3 - \delta\phi_2^3) - \left(\frac{\partial p_x}{\partial\phi_1} \frac{\partial^2 p_y}{\partial\phi_1^2} + \frac{\partial p_y}{\partial\phi_1} \frac{\partial^2 p_x}{\partial\phi_1^2} \right) \delta\phi_1 \delta\phi_2 (\delta\phi_1 - \delta\phi_2) \quad (46)$$

$$L_1 = \left[\left(\frac{\partial p_x}{\partial\phi_1} \right)^2 - \left(\frac{\partial p_y}{\partial\phi_1} \right)^2 \right] (\delta\phi_1^2 - \delta\phi_2^2) \quad (47)$$

$$L_2 = \left(\frac{\partial p_x}{\partial\phi_1} \frac{\partial^2 p_x}{\partial\phi_1^2} - \frac{\partial p_y}{\partial\phi_1} \frac{\partial^2 p_y}{\partial\phi_1^2} \right) (\delta\phi_1^3 + \delta\phi_2^3) + \left(\frac{\partial p_x}{\partial\phi_1} \frac{\partial^2 p_y}{\partial\phi_1^2} - \frac{\partial p_y}{\partial\phi_1} \frac{\partial^2 p_x}{\partial\phi_1^2} \right) \delta\phi_1 \delta\phi_2 (\delta\phi_1 + \delta\phi_2) \quad (48)$$

Similarly to the CDW case, we define $r = \delta\phi_1 + \delta\phi_2$ and $s = \delta\phi_1 - \delta\phi_2$. Expanding to the lowest order of η_S we find (for notation simplicity $L_i = L_i(r, s)$ and $K_i = K_i(r, s)$):

$$J_{\text{fluct}}^S \approx -\eta_S \left(\frac{N_{\phi_1}}{\nu_F} \right)^2 \frac{2\xi_T^{-2}}{\pi^2} \int dr \int ds \frac{(L_1 + L_2) (\xi_S^{-2} + \frac{1}{2}\xi_T^{-2} + K_1 + K_2) (1 + \mu s) r (A_1 + A_2 s)}{\left[(\xi_S^{-2} + K_1 + K_2)^2 \right] \left[(\xi_S^{-2} + \xi_T^{-2} + K_1 + K_2)^2 \right]} \quad (49)$$

$$J_{\text{fluct}}^S \approx \left[\frac{2 \langle \mathbf{v}_F^2(\phi) \rangle_\phi}{\pi} \right] \eta_S C_S \xi_T^{-2} \left\{ \ln(\xi_S^2) + \left[1 - \left(1 + \frac{\xi_T^2}{\xi_S^2} \right) \ln \left(1 + \frac{\xi_S^2}{\xi_T^2} \right) \right] \right\} \quad (50)$$

with the geometrical pre-factor:

$$C_S = - \left(\frac{N_{\phi_1}}{\nu_F} \right)^2 \frac{\left[\left(\frac{\partial p_x}{\partial\phi_1} \right)^2 - \left(\frac{\partial p_y}{\partial\phi_1} \right)^2 \right] 2(\mu A_1 + A_2) - A_1 \left[3 \left(\frac{\partial p_x}{\partial\phi_1} \frac{\partial^2 p_x}{\partial\phi_1^2} - \frac{\partial p_y}{\partial\phi_1} \frac{\partial^2 p_y}{\partial\phi_1^2} \right) - \left(\frac{\partial p_x}{\partial\phi_1} \frac{\partial^2 p_y}{\partial\phi_1^2} - \frac{\partial p_y}{\partial\phi_1} \frac{\partial^2 p_x}{\partial\phi_1^2} \right) \right]}{2 \langle \mathbf{v}_F^2(\phi) \rangle_\phi \left| \left(\frac{\partial p_x}{\partial\phi_1} \right)^2 - \left(\frac{\partial p_y}{\partial\phi_1} \right)^2 \right|^3} \quad (51)$$

Because the SDW fluctuations are only anisotropic in their momentum dependence, the geometrical pre-factor is not longer determined only by the hot-spots Fermi velocity, but also by their derivatives and the curvature of the Fermi surface near the hot spots. As a result, it is a priori not clear what the sign of C_S is. We evaluated C_S numerically using the tight binding models of Refs. [33, 39] and found $C_S = -0.25$ for Ref. [33] (with chemical potential $\mu = -1.3$) and $C_S = -0.067$ for Ref. [39] (with chemical potential $\mu = 0.1$). We also found that the negative character of C_S is robust against small changes in the chemical potential. Thus, we observe in general a tendency towards $C_S < 0$. The only situation in which we were able to find $C_S > 0$ was for Fermi surface configurations that tend to become open around (π, π) (closed near $(0, 0)$), which are not relevant for hole-underdoped compounds.

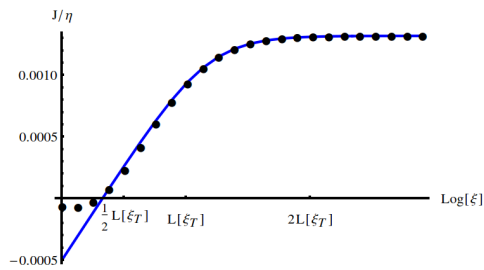


FIG. 7. Comparison of the analytic approximation to J_{fluct}^C given by Eq. (50) (solid blue line) with the numerical evaluation of the corresponding integral in Eq. (32) (black dots). For convenience, we defined $L(\xi_T) \equiv \ln(\xi_T)$.

Note that, in Eq. (50), J_{fluct}^S saturates in the regime $\xi_S \gg \xi_T$. Therefore, it is in principle possible that other contributions to J_{fluct}^S not related to the hot spots are comparable to those arising from the hot spots physics. To check this, we computed numerically Eq. (32) for the tight-binding models of Refs. [33, 39] for a range of chemical potential values. In Fig. 7 we show the specific case of the tight-binding parameters of Ref. [39] with $\mu = 0.1$, comparing it with the analytical expression given by Eq. (50). To account for the contribution that does not arise from the hot spots physics, we added a constant shift. Clearly, this additional contribution is smaller than that from the hot-spots for $\xi_S \gg 1$. We found a similar behavior when using the tight-binding parameters of Refs. [33, 39] for a variety of chemical potential values, demonstrating that Eq. (50) captures the behavior of the resistivity anisotropy in the regime where ξ_S is not too small.